EUROPEAN ORGANIZATION FOR NUCLEAR RESEARCH

RAP/afm

CERN PS/87-66 (AA)

CONFORMAL MAPPING

FOR TWO DIMENSIONAL ELECTROSTATIC BEAM POTENTIAL CALCULATIONS

Rui Alves-Pires

Geneva, Switzerland
August 1987

TABLE OF CONTENTS

		Page
1.	INTRODUCTION	1
2.	GENERAL SOLUTION USING CONFORMAL MAPPING	1
3.	APPLICATIONS TO PARTICULAR GEOMETRIES	4
	3.1 Circular Chambers	
	3.2 Rectangular Chambers	
4.	ELLIPTIC BI-GAUSSIAN BEAMS	8
	4.1 Circular Chambers	
	4.2 Rectangular Chambers	
5.	CIRCULAR BI-GAUSSIAN BEAM	11
6.	POTENTIAL AT THE BEAM CENTRE	11
	6.1 Circular Chambers	
	6.2 Rectangular Chambers	
7.	PRACTICAL COMPUTATIONS OF THE BEAM POTENTIAL	13
	7.1 The Computational Method	
8.	FINAL REMARKS	16
ACKNOWLEDGEMENTS		16
APPENDIX 1:	THE IMAGE POINTS IN A RECTANGULAR GEOMETRY	18
APPENDIX 2:	ON THE DIVERGENCE TO THE FREE SPACE POTENTIAL INTEGRAL FORMULA	21
NOTES		24
REFERENCES		25

1. INTRODUCTION

Electrostatic beam potential calculations are an important application for accelerator machines since the beam charge induced potential can play an important role in the dynamical behaviour of the beam itself. In addition, for a negatively charged beam (such as $\bar{p}$ and e^- beams), the beam space charge governs various exotic phenomena linked to the trapping of residual gas ions and charged dust particles in the beam potential wells[1]. The comprehension of these phenomena requires a precision higher than usual in the knowledge of the azimuthal potential distribution in order to know the exact location and depth of these wells.

Closed expressions for the beam potential are presented here in a generalised form, for any two dimensional geometry of boundaries (vacuum chambers at zero potential), any beam transverse charge distribution, and any beam centre location, provided that the potential created by the same beam in the free (empty) space is known. The method uses conformal mapping.

It is assumed that the treatment on the plane transverse to the beam motion is a correct approximation, and variations along the beam motion axis do not affect the results.

General results on circular and rectangular shaped vacuum chambers are given, and applications are made for bi-gaussian beams.

2. GENERAL SOLUTION USING CONFORMAL MAPPING.

The potential at any azimuthal location in the machines is assumed to be a solution of the two dimensional Poisson's equation

$$\nabla\Phi = - \frac{1}{\varepsilon_0} \varrho(x,y) \qquad (1)$$

where Φ represents the potential, $\varrho(x,y)$ is the volume charge density in the plane and ε_0 is the vacuum permittivity.

The potential must satisfy the condition $\Phi(x,y) = 0$ at the vacuum chamber walls (the boundary).

Usually the geometry involved makes the solution to the equation difficult, specially if the charge distribution and boundary geometries

are different (such as in the case of elliptic beams inside circular or rectangular vacuum chambers). In these cases, the well known method of conformal mapping can be used to find one analytical expression for the potential. This can be even easier if the chosen conformal transformation map the domain inside the boundary into one half-plane, in which case we can use the symmetry principle to determine the induced image charge distribution in the remaining half-plane. We will choose, in complex notation, the half-plane mapped by the domain inside the boundary as being $\mathrm{Im}\,(W) > 0$.

Let us denote the original plane by the z-plane, where $z = x + iy$, and the new one by the w-plane, where $w = u + iv$. Let $f : z \to w = f(z)$ denote the mapping of the z-plane onto the w-plane, and let $g : w \to z = g(w) = f^{-1}(w)$ denote the inverse mapping.

Two ways can now be used to solve the problem: either map the charge distribution into the w-plane, use the symmetry principle in order to get a solution on this plane, and map the solution back to the z-plane; or, find a solution for a space charge distribution in empty space, map it onto the w-plane, find the total solution in terms of the previous one, also using the symmetry principle, and re-map it back to the z-plane.

We will use the second way, because it does not need to calculate the map of the charge distribution, and because analytical solutions for the problem of space charge distributions in empty space exist for a wide range of distributions (such as uniform or bi-gaussian). Poisson's equation becomes, in the w-plane[2]:

$$\Delta_w \psi = -\frac{1}{\varepsilon_0}\,\sigma(w)\left|\frac{dg}{dw}\,(w)\right|^2 \qquad (2)$$

where $\psi(w) = \Phi(g(w))$ and $\sigma(w) = \varrho(g(w))$. This is still a Poisson's equation with a different charge distribution.

Suppose now that this charge distribution is in the free space, without boundaries. Let $\psi_f(w)$ (where f stands for "free") be the potential created in these conditions (the so-called free space potential). Then, using the method of images, suppose that besides the above charge

distribution we have also its induced image, with respect to the boundary. Thus, Poisson's equation will become:

$$\nabla_w \psi = - \frac{1}{\varepsilon_0} \left\{ \sigma(w) \left| \frac{dg}{dw} (w) \right|^2 - \sigma(\bar{w}) \left| \frac{dg}{dw} (\bar{w}) \right|^2 \right\} \tag{3}$$

where $\nabla_w \psi$ denotes the Laplacian of $\psi(w)$ calculated on the w-plane, and $\bar{w}$ the complex conjugate of w, its symmetrical point with respect to the boundary $Im(w) = 0$.

This extra-distribution will create an additional potential, denoted by $\psi_i(w)$, where i stands for image. It is easy to see that this additional term is related to the first one by

$$\psi_i(w) = -\psi_f(\bar{w}) \ . \tag{4}$$

The total potential is then given by

$$\psi(w) = \psi_f(w) + \psi_i(w) = \psi_f(w) - \psi_f(\bar{w}) \ , \tag{5}$$

or, expressed in other terms,

$$\Phi(z) = \Phi_f(z) - \Phi_f(z_i) \tag{6}$$

where $\Phi_f(z) = \psi_f(f(z))$ is the free space potential and $z_i = g(\bar{w})$ denotes the image of z.

The result of equation (6) is well known, saying that the potential at the point z is equal to the free space potential at z minus the free space potential at the image of z, z_i. This solution will satisfy Poisson's equation (1) inside the vacuum chamber, and the boundary condition $\Phi(z) = 0$, since on the boundary $z = z_i$ (because $w = \bar{w}$ at $Im(w) = 0$, the map of the boundary).

Thus, the problem can be easily solved if Φf is known, just by knowing the mapping functions f and g in order to calculate z_i:

$$z_i = g(\bar{w}) = g(\overline{f(z)}) \ . \tag{7}$$

3. APPLICATIONS TO PARTICULAR GEOMETRIES

3.1 Circular Chambers

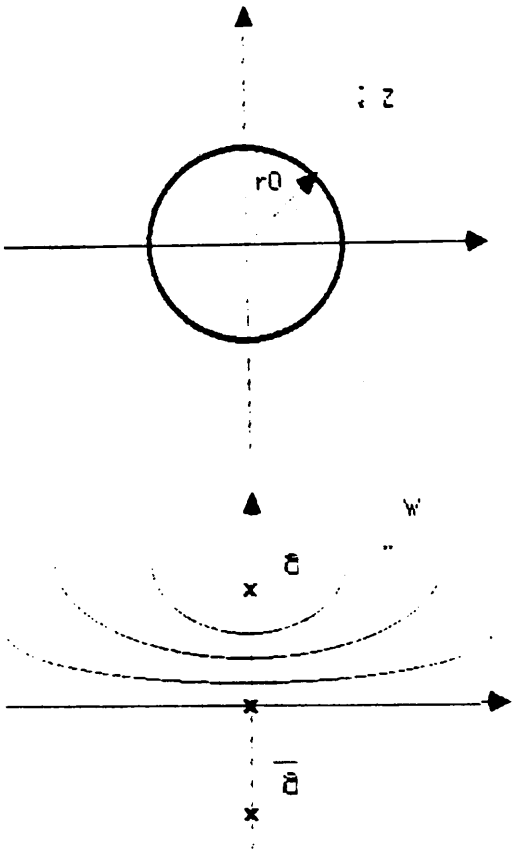

Fig. 1 - Mapping a circle.

The conformal transformation that maps a circle centered at origin ($z = 0$) and with radius r_0, in the half-plane $\mathrm{Im}(w) > 0$ (Fig. 1) is given[3] by:

$$w = f(z) = \frac{\bar{a}z - ka}{z - a} \tag{8}$$

where k and a are complex constants to be determined for each case. The inverse transformation is given by:

$$z = g(w) = k\,\frac{w - a}{w - \bar{a}}\ , \tag{9}$$

and, from equation (7) the image point will be:

$$z_i = g(\bar{w}) = k\,\frac{\overline{f(z)} - a}{\overline{f(z)} - \bar{a}} = |k|^2/\bar{z}\ .$$

Since at the boundary ($|z| = r_0$), we must have $z = z_i$, this implies $|k| = r_0$, and finally:

$$z_i = \frac{r_0^2}{\bar{z}} = \frac{r_0^2\, z}{|z|^2}\ , \tag{10}$$

or, in terms of x and y

$$x_i = \mathrm{Re}(z_i) = \frac{r_0^2 x}{x^2 + y^2}$$

$$y_i = \mathrm{Im}(z_i) = \frac{r_0^2 y}{x^2 + y^2} \tag{11}$$

which is also a well known result for the image point in a circular geometry.

3.2 Rectangular Chambers

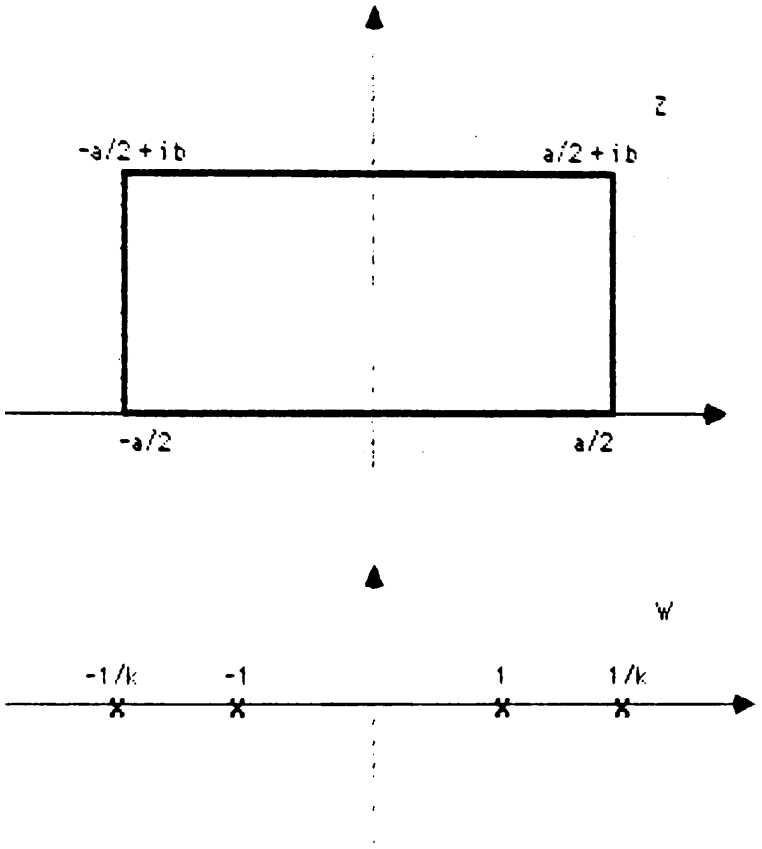

Fig. 2 - Mapping a rectangle

For rectangular chambers the problem is much more complex. The mapping of a rectangle of dimensions a * b in the upper half-plane (Fig. 2) is provided by the Jacobian elliptic function w = f(z) = sin(w/C, k) (also called elliptic sinus), where C and k are constants to be determined[3]. Its inverse is given by:

$$z = g(w) = CF(w,k) = C \int_0^w [(1 - w^2)(1 - k^2w^2)]^{-1/2} dw \qquad (12)$$

where F(w,k) denotes the incomplete elliptic integral of the first kind. k can be given[3-5] by:

$$k = \left[\frac{\theta_2(0,q)}{\theta_3(0,q)}\right]^2 = \left[\frac{2q^{1/4} \sum_{n=0}^{\infty} q^{n(n+1)}}{1 + 2 \sum_{n=1}^{\infty} q^{n^2}}\right]^2 \qquad (13)$$

where $\theta_2(u,q)$ and $\theta_3(u,q)$ are the second and third theta functions and $q = \exp(-2\pi b/a)$.

In order to find C, we note that we map the rectangle vertices $-a/2 + ib$, $-a/2$, $a/2$ and $a/2 + ib$, onto the points $-1/k$, -1, 1, $1/k$. Then we have $f(a/2) = 1$, and:

$$a/2 = g(1) = CF(1,k) = C\,K(k) \tag{14}$$

where $K(k) = F(1,k)$ is the so-called complete elliptic integral of the first kind.

Since K is completely determined by k, which, at its turn, is determined by a/b from equation (13), we can use equation (14) to determine C:

$$C = a/2K\ . \tag{15}$$

We could also show that $b = C\,K'(k)$, where

$$K'(k) = K(\sqrt{1 - k^2}) \tag{16}$$

and determine C from

$$C = b/K'. \tag{17}$$

From equation (12) we know that C is only a scaling factor, and we will do first the transformation $z \to Cz$ in order to avoid to carry C in all expressions. From equations (15) and (17) we know that the rectangle, after this transformation, will have vertices at $-K+iK'$, $-K$, K and $K+iK'$, and will be mapped onto the upper half-plane $\mathrm{Im}(w) > 0$ by $w = sn(z,k)$.

It is known that when we map a rectangle from the z-plane onto the w-plane, we will have for each point z only one corresponding point w, but the inverse is not true, that is, for each point w we will have an infinity of corresponding points in the z-plane, because of the dependence on the integration path of the integral appearing in equation (12).

It can be shown[6] that if z is a possible value for F(w,k) for one integration path, so are any points with the form:

$$4nK + 2mK'i + z$$

or (18)

$$4nK + 2mK'i + 2K - z$$

where n and m are any integers (positive or negative).

This result and that of their images (expression A.10, Appendix 1), has a great physical meaning, which can be seen using the symmetry principle (see, for example ref. 7, p. 399).

Taking the rectangle (1) in Fig. 3 mapped onto Im(w) > 0, it follows from the symmetry principle that any reflection over its boundaries will map the reflection of Im(w) > 0 over the u-axis, which is Im(w) < 0. Thus, rectangles (2) and (4) are both maps of Im(w) < 0 because they are obtained from (1), by reflection respectively over I and II. Analytically, these new rectangles are generated by the transformations $z \to \bar{z}$ and $z \to 2K - \bar{z}$. The rectangle (3), obtained by a reflection of either (2) or (4), will then be a map of Im(w) > 0. Analytically it is generated from (1) by the transformation $z \to 2K - z$.

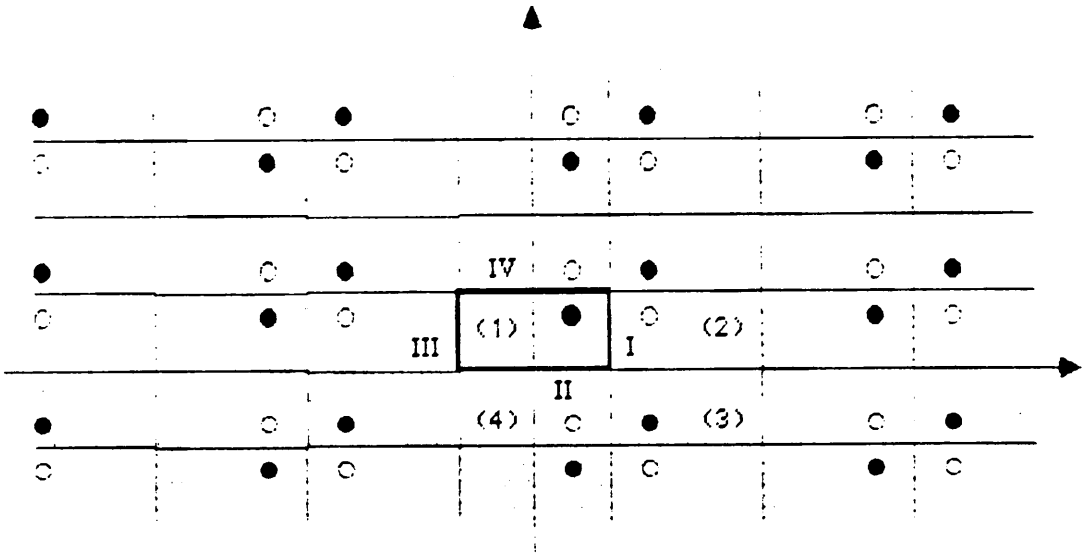

Fig. 3 - The periodicity of the Jacobian elliptic functions.

By extending this to the whole plane, we will obtain a set of rectangles covering it, and generated from (1) by the complex transformations (18) and (A.10). Those generated from (18) will be maps of Im(w) > 0, and those from (A.10) maps of Im(w) < 0. The rectangle (1) boundaries

will behave as two sets of parallel mirrors giving an infinity of images, and of reflections of the images.

In our calculations, we must take into account all these images and reflections of the images. Thus, expression (6) becomes, for this particular case:

$$\Phi(z) = \sum_{n,m} [\Phi_f(4nK + 2mK'i + z) + \Phi_f(4nK + 2mK'i + 2K - z) - \Phi_f(4nK + 2mK'i + \bar{z}) - \Phi_f(4nK + 2mK'i + 2K - \bar{z})] \tag{19}$$

where the sums are extended to all possible integer values of n and m.

Here, we note that it is necessary to return to our original coordinate system, multiplying the variables with the scaling factor C. Doing this, the above expression becomes, in terms of x and y:

$$\Phi(n,y) = \sum_{n,m} [\Phi_f(2na+x,\ 2mb+y) + \Phi_f(2na+a-x,\ 2mb-y) - \Phi_f(2na+x,\ 2mb-y) - \Phi_f(2na+a-x,\ 2mb+y)] \ . \tag{20}$$

4. *ELLIPTIC BI-GAUSSIAN BEAMS*

An elliptic bi-gaussian charge distribution, centered at point (x_c, y_c) and with r.m.s. sizes σ_x and σ_y ($\sigma_y \neq \sigma_x$ in order to be elliptic), has a charge density given by:

$$\varrho(x,y) = \frac{\lambda}{2\pi\ \sigma_x\sigma_y} \exp\left[- \frac{(x - x_c)^2}{2\sigma_x^2} - \frac{(y - y_c)^2}{2\sigma_y^2} \right] \tag{21}$$

where λ is the linear charge density:

$$\lambda = \iint_S \varrho(x,y)\ dS \ . \tag{22}$$

The corresponding free space potential is given[8,9] by:

$$\Phi_f(x,y) = \frac{\lambda}{4\pi\varepsilon_0} \int_0^{\infty} \frac{\exp[-((x - x_c)^2/(2\sigma_x^2 + q)) - ((y - y_c)^2/(2\sigma_y^2 + q))]}{\sqrt{(2\sigma_x^2 + q)(2\sigma_y^2 + q)}}\, dq \tag{23}$$

Following Appendix 2, we will use instead the expression (B.4)

$$\Phi_f(x,y) = \frac{\lambda}{2\pi\varepsilon_0} \int_r^1 \frac{\exp[-(1 - t^2)(A + B/t^2)]}{1 - t^2} \tag{24}$$

with

$$A(x) = \frac{(x - x_c)^2}{2(\sigma_x^2 - \sigma_y^2)}$$

$$B(y) = \frac{(y - y_c)^2}{2(\sigma_x^2 - \sigma_y^2)} \tag{25}$$

$$r = \frac{\sigma_y}{\sigma_x}$$

4.1 Circular Chambers

Application of equations (6) and (10) or (11) and (24) will give, for the potential created by an elliptic bi-gaussian beam inside a circular vacuum chamber:

$$\Phi(x,y) = \frac{\lambda}{2\pi\varepsilon_0} \int_r^1 \frac{\exp[-(1 - t^2)(A + B/t^2)] - \exp[-(1 - t^2)(A^* + B^*/t^2)]}{1 - t^2}\, dt \tag{26}$$

where $A(x)$ and $B(y)$ are given by equations (25) and $A^*(x,y) = A(x_i)$, $B^*(x,y) = = B(y_i)$ are the same functions calculated at the image point.

4.2 Rectangular Chambers

According to expressions (20) and (24), the potential for a rectangular chamber is:

$$\Phi(x,y) = \frac{\lambda}{2\pi\varepsilon_0} \sum_{n,m} \int_r^1 \{\exp[-(1 - t^2)(A_n + B_m/t^2)] +$$

$$+ \exp[-(1 - t^2)(A_n^* + B_m^*/t^2)] - \exp[-(1 - t^2)(A_n^* + B_m/t^2)] -$$

$$- \exp[-(1 - t^2)(A_n + B_m^*/t^2)]\}dt/(1 - t^2)$$

or

$$\Phi(x,y) = \frac{\lambda}{2\pi\varepsilon_0} \sum_{n,m} \int_r^1 \{\exp[-(1 - t^2)A_n] - \exp[-(1 - t^2)A_n^*]\} \cdot$$

$$\cdot \{\exp[-(1 - t^2)B_m/t^2] - \exp[-(1 - t^2)B_m^*/t^2]\}dt/(1 - t^2) \qquad (27)$$

where

$$A_n = \frac{(2na + x + x_c)^2}{2(\sigma_x^2 - \sigma_y^2)} \quad , \qquad B_m = \frac{(2mb + y - y_c)^2}{2(\sigma_x^2 - \sigma_y^2)} \qquad (28)$$

and

$$A_n^* = \frac{(2na + a - x - x_c)^2}{2(\sigma_x^2 - \sigma_y^2)} \quad , \qquad B_m^* = \frac{(2mb - y - y_c)^2}{2(\sigma_x^2 - \sigma_y^2)} \; . \qquad (29)$$

The sums are extended to all the possible integer values of n and m.

5. *CIRCULAR BI-GAUSSIAN BEAM*

When $\sigma_x = \sigma_y = \sigma$, we will use expression (B.8) for the free space potential created by a bi-gaussian beam centered at (x_c, y_c).

$$\Phi_f(x,y) = \frac{\lambda}{4\pi\varepsilon_0} \int_0^k \frac{\exp(-r^2 t)}{t}\, dt \tag{30}$$

with

$$k = 1/2\sigma^2$$
$$r^2 = (x - x_c)^2 + (y - y_c)^2 \ . \tag{31}$$

Applications to particular geometries are easy to perform, with the expressions (6) and (10) (for circular geometries) or (20) (for rectangular geometries).

6. *POTENTIAL AT THE BEAM CENTRE*

Since the maximum of the potential is usually approximately at the beam centre (this is exactly true for a beam in empty space, and it is not so different if the beam dimensions are much smaller than the distances to the vacuum chamber walls), it is useful to calculate the potential at $x = x_c$, $y = y_c$ (the beam centre).

6.1 Circular Chambers

For an elliptic bi-gaussian beam, we will obtain,

$$\Phi(x_c, y_c) = \frac{\lambda}{2\pi\varepsilon_0} \int_r^1 \frac{1 - \exp[-(1 - t^2)(A + B/t^2)]}{1 - t^2}\, dt \tag{32}$$

where

$$A = Cx_C^2$$

$$B = Cy_C^2 \qquad (33)$$

$$C = \frac{(r_0^2/r_C^2 - 1)^2}{2(\sigma_x^2 - \sigma_y^2)}$$

$$r_C^2 = x_C^2 + y_C^2$$

For a circular bi-gaussian beam, the expression is

$$\Phi(x_C,y_C) = \frac{\lambda}{2\pi\varepsilon_0} \int_0^k \frac{1 - \exp(-r^2t)}{t}\, dt \qquad (34)$$

where

$$r^2 = (r_0^2/r_C^2 - 1)^2 \cdot r_C^2 \qquad (35)$$

6.2 Rectangular Chambers

The expression for the potential at the beam centre for an elliptic bi-gaussian charge distribution is the same as (28), but with:

$$A_n = \frac{2n^2a^2}{\sigma_x^2 - \sigma_y^2} \quad , \qquad B_m = \frac{2m^2b^2}{\sigma_x^2 - \sigma_y^2} \qquad (36)$$

$$A_n^* = \frac{(2na + a - 2x_C)^2}{2(\sigma_x^2 - \sigma_y^2)} \quad , \qquad B_m^* = \frac{2(mb - y_C)^2}{\sigma_x^2 - \sigma_y^2} \quad .$$

For a circular bi-gaussian charge distribution, we will have: (37)

$$\Phi(x_C,y_C) = \frac{\lambda}{4\pi\varepsilon_0} \sum_{n,m} \int_0^K [\exp(-A_nt)-\exp(-A_n^*t)] \cdot [\exp(-B_mt)-\exp(-B_m^*t)]\, \frac{dt}{t}$$

where

$$A_n = 4n^2a^2 \quad , \qquad B_m = 4m^2b^2$$
$$A_n^* = (2na + a - 2x_c)^2 \quad , \qquad B_m^* = 4(mb - y_c)^2 \tag{38}$$

7. *PRACTICAL COMPUTATIONS OF THE BEAM POTENTIAL*

A FORTRAN code, in a subroutine form, has been written to calculate the beam potential from equations (26) and (28). Its input parameters are:

(x,y) the point where potential is to be calculated,
(x_c,y_c) the beam centre,
σ_x,σ_y the beam r.m.s. sizes,
a_H,a_V the chamber total horizontal and vertical dimensions ($a_H=a_V=2r_0$ for circular chambers, and $a_H=a$ and $a_V=b$ for rectangular ones),
C the circular chamber shape, or
R the rectangular chamber shape,
λ/e the number of particles per metre, where λ is the linear charge density (22) and e is the electronic charge,
the maximum value of $|n|$ and $|m|$ in formula (28).

The coordinates (x, y, x_c and y_c) are referred to the vacuum chamber centre.

Tests of the routine were made using data from the output of APERTURE[10], BEPO DATA. At the time of the tests, the BEPO DATA file provided the parameters for the beam potential calculations for 298 points along the AA machine. The calculations were made at the beam centre position (x_c,y_c).

In order to make sure of the results, another program based on bi-dimensional Fourier series for rectangular chambers was also provided. It used the expression:

$$\Phi(x,y) = D \sum_{n,m=1}^{\infty} C_{nm} \sin(n\pi x/a_H) \sin(m\pi y/a_V) \tag{39}$$

where

(x,y) is the point where the potential is to be calculated,

$D = 2\lambda/\pi^3\varepsilon_0\sigma_x\sigma_y$,

$C_{nm} = A_nB_m/[(n/a_H)^2 + (m/a_V)^2]$,

$$A_n = (1/a_H)\int_0^{a_H} \exp[-(x - x_c)^2/2\sigma_x^2]\sin(n\pi x/a_H)\,dx, \tag{40}$$

$$B_m = (1/a_V)\int_0^{a_V} \exp[-(y - y_c)^2/2\sigma_y^2]\sin(m\pi y/a_V)\,dy. \tag{41}$$

In equations (39) to (41) the coordinates refer to the lower left corner of the rectangle.

The maximum value of n and m was set to 8000, and the convergence criterium used was that the ratios $|A_{2n}/A_2|$, $|A_{2n+1}/A_1|$, $|B_{2m}/B_2|$ and $|B_{2m+1}/B_1|$ should be lower than 10^{-6}.

For most of the 298 points (actually for 226) the required convergence criterium was not filled.

In order to compare the output from the two programs, all the vacuum chambers were supposed rectangular. The comparison was made using

$$\eta = \left|\frac{\Phi_1 - \Phi_2}{\Phi_1}\right| \tag{42}$$

where

Φ_1 is the potential calculated by the subroutine,

Φ_2 is the potential calculated from the Fourier series.

The results were:

- For 74 of the 298 points, η was higher than 100% and lower than 12% for the other 224. This was clearly due to the non-convergence of the Fourier series (all of those 74 points were considered non-convergent).

- For the 72 convergent points, η was lower than 0.3% for 67 of them and between 0.5% and 1.6% for the remaining five (Table 1).

Table 1

Azimuthal position (m)	η-variation (%)	Azimuthal position (m)	η-variation (%)
0.000			
0.906	-0.0354	73.714	0.0331
0.906	-0.0100	73.714	0.2695
1.007	-0.0144	75.477	0.1500
1.964	0.0015	75.528	0.0269
2.064	0.1571	76.132	0.0191
2.266	-0.0211	76.132	0.1183
2.316	-0.0195	78.448	-0.0396
5.438	0.0032	78.498	-0.0063
5.539	0.0752	79.001	-0.0125
5.790	0.6731	79.053	-0.0200
5.891	0.7046	80.260	0.0455
6.470	-0.0015	80.260	-0.0041
6.571	1.1588	83.483	0.0162
6.797	1.1376	83.483	0.0515
6.797	-0.0028	84.490	0.0687
6.896	0.1460	84.490	0.0103
7.296	0.1345	85.296	0.0017
7.880	0.0896	85.296	0.1129
8.056	0.0226	87.839	-0.0977
8.862	0.0168	89.675	0.1082
9.667	-0.0564	92.445	0.0472
10.272	-0.0954	137.662	0.1277
10.674	-0.1161	138.669	0.0960
11.581	-0.1766	142.344	0.2146
13.696	0.1819	143.754	0.0910
15.383	0.2975	144.912	0.1144
61.932	0.0925	146.851	-0.1263
66.615	1.6345	149.543	0.1201
68.629	0.1551	149.543	0.0454
71.297	-0.1323	150.350	0.0652
71.297	0.1176	150.350	0.0571
72.103	0.0030	154.479	0.0036
72.103	0.0099	154.479	0.2002
72.809	0.0641	155.637	0.0093
72.809	0.0565	155.737	0.0021
	0.0357	156.492	0.0021

A complete test should also include circular chambers and comparison with other methods. For this purpose, another program using a linear finite element method was tested, but it provided η-values of the order of 10 to 20%, and the convergence was very slow.

7.1 The Computational Method

The integrations in formulae (28) and (39) were made using a CERN Library program (CHEBQU, see note 1), which also provides an estimate of the relative error. It was always lower than 10^{-6} for the checked values.

The maximum values of |n| and |m| in formula (27) were varied between 4 and 10, and the variations in the results were in the order of 1 to $2^0/_{00}$.

Also for formula (27) the sums were performed before the integration since for large enough values of |n| and |m|, the exponentials become equal inside each parenthesis and the integration function is approximately zero. The result of the integration of a zero function is a floating point divided exception. (The same is true even when using other CERN program library integration routines). Sometimes, even for |n| or |m| equal to 2 or 3 the exception appeared, and sometimes for higher values, which does not enable the determination of a maximum summation value for all cases. Summation before integration avoids these problems.

The subroutine showed to be fast. The total CPU time used for the computation of the potential at the beam centre for all the 298 points was about 2 minutes. Compared with the Fourier series or the finite element methods, this is about 10 to 20 times faster.

8. FINAL REMARKS

Since this was a work on beam potential and not a treat on elliptic functions, some points on that matter may seem obscure, specially where proofs are not given in a complete way. I am sure that the reader can have a better understanding on that matter by studying the abundant literature published on elliptic functions, in particular those listed as references [4] (for a summary of general results), and [5], [6], [11], [12], [13] (for more detailed descriptions). Those listed as [2], [3] and [7] have several chapters on conformal mapping, including circles and rectangles, and on elliptic functions. Reference [3], p. 719, has an application for a point charge inside a rectangle.

ACKNOWLEDGEMENTS

I would like to thank J.M. Alberty for his initial idea on that matter, and for his helpful comments and discussions. I am indebted to A. Poncet and F. Pedersen for their comments, suggestions and discussions, specially on the physical meaning of the problem and results.

C. Gaspar made all the drawings.

APPENDIX 1

THE IMAGE POINTS IN A RECTANGULAR GEOMETRY

In order to get $z_i = F(\bar{w},k)$, we will express the incomplete integral of the first kind with a complex argument

$$F(w,k) = \int_0^w [(1 - w^2)(1 - k^2w^2)]^{1/2}\, dw \qquad (A.1)$$

as a sum of two of such integrals with real arguments. Using the change of the variable of integration

$$w = \sin\theta \qquad (A.2)$$

we will obtain

$$F(w,k) = F(\theta,m) = \int_0^\theta [1 - m \sin^2\theta]^{1/2}\, d\theta \qquad (A.3)$$

where $m = k^2$ (we will use $\underline{k}$ when the variable of integration is w and m when it is θ).

If w is real but $|w| > 1$, or if it is not real, the angle θ will not be real:

$$\theta = \varphi + i\psi\ . \qquad (A.4)$$

Using the properties of the sine function with complex argument

$$w = \sin\theta = \sin(\varphi+i\psi) = \sin\varphi\ \mathrm{ch}\psi + i\ \cos\varphi\ \mathrm{sh}\psi = u + iv \qquad (A.5)$$

it is possible to determine φ and ψ. When $u \neq 0$ and $v \neq 0$:

$$tg^2\varphi = \frac{u^2 - v^2 - 1 + \sqrt{(u^2 - v^2 - 1) + 4u^2v^2}}{2v^2}$$

$$th\psi = \frac{v}{u}\, tg\varphi \ . \qquad (A.6)$$

φ is determined less than a sign and an integer multiple of π. It must be only such that $\sin\varphi$ has the same sign as u (from A.5), and $\cos\varphi$ is positive (from the second expression of A.6, knowing from A.5 that $th\psi$ and v have the same sign). This is not important since, as we shall see, we only use the square of its trigonometrical functions.

φ and ψ being known, the integral (A.3) can be calculated[4] from:

$$F(\varphi+i\psi,m) = F(\lambda,m) + iF(\mu,1-m) \qquad (A.7)$$

where $cotg^2\lambda$ is the positive root of

$$x^2 - [cotg^2\varphi + m\, sh^2\psi/\sin^2\varphi - 1 + m]x - (1 - m)\, cotg^2\varphi = 0 \qquad (A.8)$$

and

$$m\, tg^2\mu = tg^2\varphi\, cotg^2\lambda - 1 \ . \qquad (A.9)$$

In this case, there is an important uncertainty in λ and μ, since both are determined to be less than an integer multiple of π and a sign. In order to get an expression for an image point of z, we will reduce the possible values of λ and μ to eliminate this uncertainty, which is the same as to reduce the map of the w-plane into some closed domain of the z-plane, which we choose to be the original rectangle and another one obtained from the first by symmetry over the x-axis.

Imposing a map of $Re(w) > 0$, $Im(w) > 0$ onto the right-hand side of the original rectangle, of $Re(w) < 0$, $Im(w) > 0$ onto its left-hand side, of $Re(w) > 0$, $Im(w) < 0$ onto the right-hand side of another rectangle created by symmetry of the first one over the x-axis, and of $Re(w) > 0$, $Im(w) < 0$ onto the left-hand side, we will impose them to satisfy $-\pi/2 < \lambda, \mu \leq \pi/2$ (that is, they will be determined by applying directly

the functions arccotg and arctg over the results from A.8 and A.9), and in such a way that λ has the same sign as u, and μ the same sign as v.

If w is a map of a point z inside the original rectangle and if we determine, as above, λ and μ from $w = u+iv$, such that $z = F(w,k) = F(\lambda,m) + iF(\mu,1-m)$, we can determine

$$z_i = F(\bar{w},k) = F(u-if,k) \;) \; f(\lambda,m) + iF(-\mu,1-m)$$

since μ changes sign with v. Using the property $F(-\theta/m) = -F(\theta/m)$, we will have finally

$$z_i = F(\lambda,m) - iF(\mu,1-m) = \bar{z} \; . \qquad (A.10)$$

Thus, $\bar{z}$ is one image point of z. A similar result could be obtained for the cases $u = 0$ or $v = 0$.

If u is one of the possible values for $F(w,k)$, for a certain w, and $\bar{z}$ one of the possible values for $F(\bar{w},k)$, the set of points with the form

$$4nK + 2mK'i + \bar{z}$$

or (A.11)

$$4nK + 2mK'i + 2K - \bar{z}$$

will be (from expressions (18) in the text) the set of all possible values of $F(\bar{w},k)$.

The ubiquity of the incomplete elliptic integrals of the first kind, expressed in (18) and (A.11) is also a consequence of the uncertainty of the definitions of λ and μ, which are, as already said, defined to be less than an integer multiple of π and a sign. We will only note[4] that:

$$F(n\pi\pm\lambda,m) = 2nK \pm F(\lambda,m)$$

(A.12)

$$F(n'\pi\pm\mu,1-m) = 2n'K' \pm F(\mu,1-m)$$

but the problem is rendered more complex since λ and μ being defined as above, not all combinations of $n\pi\pm\lambda$ and $n'\pi\pm\mu$ are valid but only those which combine $2n\pi+\lambda$ with $n'\pi+\mu$ or $(2n+1)\pi-\lambda$ with $n'\pi-\mu$. For the set of all possible values of $F(w,k)$ this will also give the result (18), or (A.11), for the images.

APPENDIX 2

ON THE DIVERGENCE OF THE FREE SPACE POTENTIAL INTEGRAL FORMULA

The free space potential created by a bi-gaussian charge distribution centered at (o,o) is given[8,9] by:

$$\Phi_f(x,y) = \frac{\lambda}{4\pi\varepsilon_0} \int_0^\infty \frac{\exp[-(x^2/(2\sigma_x^2 + q)) - (y_x^2/(2\sigma^2 + q))]}{\sqrt{(2\sigma_x^2 + q)(2\sigma_y^2 + q)}}\, dq \qquad (B.1)$$

By changing the integration variable[7]:

$$t = \left(\frac{2\sigma_y^2 + q}{2\sigma_x^2 + q}\right)^{1/2} \qquad (B.2)$$

with

$$r = \frac{\sigma_y}{\sigma_x}$$

$$A(x) = \frac{x^2}{2(\sigma_x^2 - \sigma_y^2)} \qquad (B.3)$$

$$B(y) = \frac{y^2}{2(\sigma_x^2 - \sigma_y^2)} \quad ,$$

and supposing σ_x different from σ_y, we obtain the new expression for (B.1):

$$\Phi_f(x,y) = \frac{\lambda}{2\pi\varepsilon_0} \int_r^1 \frac{\exp[(t^2 - 1)(A + B/t^2)]}{1 - t^2}\, dt \qquad (B.4)$$

The integrant function has one singularity in one of the extremes of the integration interval (at t = 1), and its limit when $t \to 1$ is ∞.

In order to perform the integration, we will remove the singularity by subtracting from (B.4) another integral which does not depend on x and y, still satisfying Poisson's equation,

$$\frac{\lambda}{2\pi\varepsilon_0}\int_r^1 \frac{dt}{1 - t^2} \qquad (B.5)$$

and we will obtain:

$$\Phi_f(x,y) = \frac{\lambda}{2\pi\varepsilon_0}\int_r^1 \frac{\exp[(t^2 - 1)(A + B/t^2)] - 1}{1 - t^2}\, dt \quad . \qquad (B.6)$$

From now, the integrant function has a removable singularity at t = 1 (its limit when t → 1 is -a-b, a finite value), and the integration interval being finite, the integral will be convergent.

Since (B.4) is the sum of (B.5) with (B.6), (B.5) is well known as being divergent, and (B.6) has been shown to be convergent, (B.4) must be divergent. Then, for practical purposes, the expression (B.6), or its correspondent in q-integration, must be used instead of (B.4). The integration in t is also simpler than in q, since the integrant function is simpler, known A(x) and B(y), and the integration interval is finite. Additionally, it will allow a simpler expression for the free space potential for rectangular boundaries.

The additional term (B.5), independent of x and y, is not important in electric field calculations, since it will disappear when differentiating with respect to x or y, or in calculations of differences of potential. Expressions (B.4) and (B.6) are then equivalent.

The above transformation (B.2) is meaningless if $\sigma_x = \sigma_y = \sigma$, and we will provide a new transformation:

$$t = \frac{1}{2\sigma^2 + q} \qquad (B.7)$$

then, (B.1) becomes

$$\Phi_f(x,y) = \frac{\lambda}{4\pi\varepsilon_0} \int_0^k \frac{\exp(-r^2t)}{t}\, dt \qquad (B.8)$$

where

$$k = 1/2\sigma^2$$

$$r^2 = x^2 + y^2 \ . \qquad (B.9)$$

Using the same arguments as for the case $\sigma_x \neq \sigma_y$, we could prove that this integral is also divergent. An equivalent convergent form could be:

$$\Phi_f(x,y) = \frac{\lambda}{4\pi\varepsilon_0} \int_0^k \frac{\exp(-r^2t) - 1}{t}\, dt \qquad (B.10)$$

and the additional term is also unimportant for electric field or differences of potential calculations.

NOTES

[1] FORTRAN routines for the calculation of the θ-functions and the complete integrals of the first kind are available at CERN, namely the programs ELLICK (KERNLIB library, program C308, by K.S. Kölbig) for complete elliptic integrals and THETA1 (GENLIB library, program C314, by H.-H. Umstätter) for θ-functions.

[2] The FORTRAN program ELIN1 (GENLIB library, program C319, by H.-H. Umstätter) computes the incomplete elliptic integral of the first kind F(x,k), for $-1 \leq x \leq +1$.

Programs also exist for the computation of the Jacobian elliptic function, either with real or complex arguments, namely ELFUN and CELFUN (GENLIB library, programs C318 and C319, by H.-H. Umstätter). These routines compute the three functions sn(w,k), Cn(w,k) and dn(w,k), for w real (ELFUN) or complex (CELFUN). Restrictions are made for the arguments: $|Re(w)| \leq 3K$, $|Im(w)| \leq 3K'$. Outside this range, the precision is lower, and the signs of the functions can become incorrect.

[3] CHEBQU, Double-Precision Clenshaw-Curtis Integration. Author: T. Havie. GENLIB.CERN program library, program D115. Computes integrals using the modified Clenshaw-Curtis algorithm, written as an ordinary quadrature formula. The routine is fast and stable with respect to accumulation of round-off errors, when a very high precision is wanted[14].

REFERENCES

1. F. Pedersen and A. Poncet, Proton-Antiproton Instability in the AA, PS/AA/ME Note 81, March 1985.

2. P. Henrici, Applied and Computational Complex Analysis, Vol. 1, p. 372, John Willey and Sons, New York, 1974.

3. M. Lavrentiev and B. Chabat, Méthodes de la Théorie des Fonctions d'une Variable Complexe, MIR, Moscou, 1977.

4. M. Abramowitz and I.A. Stegun (Editors), Handbook of Mathematical Functions, National Bureau of Standards, Washington, 1964.

5. A. Eagle, The Elliptic Functions as They Should Be, Galloway and Porter, Cambridge, 1958.

6. E.H. Neville, Jacobian Elliptic Functions, Clarendon Press, Oxford, 1951.

7. B.A. Fuks and B.V. Shabat, Functions of a Complex Variable and Some of Their Applications, Vol. 1, Pergamon Press, London, 1964.

8. B. Houssais, Private Communication (Univ. de Rennes, 1967), referred to by B.W. Montague in Calculation of Luminosity and Beam-Beam Detuning in Coasting-Beam Interaction Region, CERN-ISR-GS/75-36, 1975.

9. S. Kheifets, Potential of a Three-Dimensional Gaussian Bunch, PETRA Note 119, 1.10.1976, referred to by M. Bassetti and G.A. Erskine in Closed Expressions for the Electric Field of a Two Dimensional Gaussian Bunch, CERN-ISR-TH/80-06, 1980.

10. R. Alves Pires, APERTURE - A Computer Program to Represent Beam Dimensions and Machine Apertures in Circular Accelerators, CERN/PS/87-65 (AA), 1987.

11. F. Bowman, Introduction to Elliptic Functions with Applications, English Universities Press, London, 1953.

12. A. Cayley, Elliptic Functions, Dover Publications, New York, 1961.

13. A. Erdelyi (Editor) and H. Bateman, Higher Transcendental Functions, Vol. 2, McGraw Hill, New York, 1953.

14. T. Havie, On a Modification of the Clenshaw-Curtis Quadrature Formula, BIT (9), 338-350, 1969.
    T. Havie, Some Methods for Automatic Integration and Their Implementation on the CERN CDC 65/66000 Computers, CERN Report 71-26, 1971.
    T. Havie, Further Remarks on the Modified Clenshaw-Curtis Quadrature Formula, Internal Report, DD/71/21, 1971.